RSC Advances

PAPER

View Article Online
View Journal | View Issue

Cite this: *RSC Adv.*, 2019, **9**, 7620

Silicon/nitrogen synergistically reinforced flame-retardant PA6 nanocomposites with simultaneously improved anti-dripping and mechanical properties†

Shuo Fan,[ab] Ruchao Yuan,[ab] Dequn Wu,[*ab] Xueli Wang,[c] Jianyong Yu[c] and Faxue Li[*ab]

Received 17th December 2018
Accepted 13th February 2019

DOI: 10.1039/c8ra10325a

rsc.li/rsc-advances

A facile route of 'copolymerization/blending' was proposed to fabricate silicon/nitrogen synergistically reinforced flame-retardant PA6 nanocomposites with simultaneously improved anti-dripping and mechanical properties. Firstly, a persistently inherent flame-retardant PA6 (FR-PA6), with 1,3-bis(3-aminopropyl)tetramethyl disiloxane (MSDS), was synthesized *via* controllable amidation and a polycondensation reaction. Melamine cyanurate (MCA) nanoparticles as a 'gas phase' synergistic agent were then added into FR-PA6 to further improve its flame retardancy. The primarily obtained FR-PA6 could be extinguished after a few melt droplets dropped as ignited, and passed the V-2 rating with enhanced mechanical properties, while PA6 had no rating (NR). The prepared FR-PA6/MCA nanocomposites could attain a limiting oxygen index (LOI) value of 32.7%, and passed the V-0 level with only 1 melting droplet with similar mechanical properties to PA6. Accordingly, the special 'condensed-gas phase' synergistic flame-retardant mechanism of FR-PA6/MCA nanocomposites was proposed through studying the residues and pyrolysis volatiles. This work provided a facile route as a model for developing functional PA6 for diverse engineering applications.

Introduction

As one of the most versatile engineering materials, polyamide 6 (PA6) is widely used in several fields. However, PA6 is an extremely flammable polymer with a fast flame propagation speed, high heat release and serious melt dripping, which greatly limit its application in many specific fields.[1,2] Therefore, it is important to develop a flame-retardant PA6 with high performance. Copolymerization, *in situ* polymerization and blending are three classic methods to prepare flame-retardant materials.[3–5] The latter two methods are most commonly used due to the features of convenience, efficiency and easy processability, but the defects, such as terrible dispersion, poor incompatibility and significant deterioration of mechanical properties, cannot be ignored.[6] By contrast, the above terrible issues are easily covered by the first method.[7–9] However, the complicated implementation process of copolymerization always consumes much labor power and financial capacity. Thus the combined method of 'polymerization/blending' is a research hotspot in engineering applications.

Silicon-containing flame retardants with excellent thermal stability, non-toxic and eco-friendly performance are becoming new potential candidates for non-halogen flame retardants.[10–13] Therein, polydimethylsiloxane (PDMS) with high heat resistance and thermal stability is one of the most popular organosilicone flame retardants.[14–16] During combustion, a compact stable superficial carbonaceous-silicate layer can be formed on the surface of the matrix by PDMS to insulate the underlying matrix from the external radiative combustible environment and restrain the polymer melts from dripping. Besides, the released silicon pyrolysis volatiles of PDMS are also conducive to diluting combustible gases and stabilizing the carbon layer. But the defect of PDMS is that the functional hydroxyl groups attached to silicon are prone to self-dehydration rather than reacting with other polymers. Thus 1,3-bis(3-aminopropyl) tetramethyldisiloxane (MSDS) as a common derivative of PDMS with two terminal amine groups is picked to develop a persistently flame-retardant system. Liao *et al.*[17] used MSDS to prepare a novel phosphorus–nitrogen–silicon polymeric flame retardant, and the results showed that the MSDS was efficient to enhance the flame retardancy.

Considering the cost rate and efficiency, nitrogen-rich melamine cyanurate (MCA) nanoparticles formed by melamine (ME) and cyanuric acid (CA) *via* hydrogen bonding may be

[a]Key Laboratory of Textile Science & Technology, Ministry of Education, College of Textiles, Donghua University, Shanghai 201620, China. E-mail: fxlee@dhu.edu.cn
[b]College of Textiles, Donghua University, Shanghai 201620, China
[c]Innovation Center for Textile Science & Technology, Donghua University, Shanghai 201620, China

† Electronic supplementary information (ESI) available: Typical data from DSC, TG, XRD and Py-GC/MS data, real-time images of FR-PA6/MCA composites. See DOI: 10.1039/c8ra10325a

an effectively synergistic flame retardant for MSDS in the gas phase.[18–20] MCA can be thermally degraded into high heat-insulating products through a deammoniation reaction with huge amounts of heat absorbed and large volumes of incombustible ammonia gases being released, which can dilute the concentration of combustible gases and lower the surrounding temperature. So MCA can be regarded as the synergistic agent for silicon in forming a 'condensed-gas phase' barrier.

In this work, silicon-containing inherent FR-PA6 copolymers were first synthesized by introducing MSDS into PA6 backbones *via* an amidation reaction. MCA nanoparticles as synergistic additive flame retardants were then added to the FR-PA6 pre-polymers *via in situ* polymerization to prepare FR-PA6/MCA nanocomposites. The chemical structures, thermal stability, mechanical properties and combustion mechanism of the prepared products were intensively investigated. The results showed that MSDS and MCA nanoparticles played an extremely synergistic role in improving the flame retardancy, anti-dripping and mechanical properties of PA6.

Experimental section

Materials

ε-Caprolactam (CPL, 99%), adipic acid (AC, 99%) and amino-caproic acid (AA, 99%) were purchased from Aladdin (Shanghai, China). Melamine cyanurate nanoparticles (MCA, 98%, 800 ± 20 nm), 1,3-bis(3-aminopropyl)tetramethyldisiloxane (MSDS, 99%) and dimethylsulfoxide-d_6 (DMSO-d_6) were supplied by Alfachem. Co., Ltd. (Zhengzhou, China). All the materials were used as received.

Synthesis of FR-PA6 copolymers

FR-PA6 copolymers were prepared by two-step polymerization (Fig. 1). A 500 mL stainless steel reactor, equipped with a mechanical stirrer and a nitrogen flow device, was charged with 200 g (1.77 mol) CPL, 12.85 g (0.088 mol) AC, 10 g (0.56 mol) water and 2 g (0.015 mol) AA. After purging with nitrogen, the reactor was heated to 260 °C for 2 h with a pressure of 0.2 MPa. The pressure was decreased for polymerization for about 1.5 h, and then the binary carboxyl terminated PA6 (PA6-COOH) oligomer was prepared. Subsequently, 21.83 g (0.088 mol) MSDS was added into the reactor at 200 °C, and the temperature was heated to 240 °C for 2 h (PA6-MSDS pre-polymer). Afterward, the reactor was set to 200 Pa pressure until the FR-PA6 with high viscosity was synthesized. The FR-PA6 copolymers with different weight contents of MSDS were listed in Table 1.

Preparation of FR-PA6/MCA nanocomposites

A 250 mL three-necked round bottom flask equipped with a mechanical stirrer and a nitrogen flow device was charged with 150 g PA6-MSDS pre-polymer and 9 g (6 wt%) MCA (Fig. 1), and then the flask was heated to 240 °C and maintained for 4 h. Finally, the FR-PA6/MCA-6 with high viscosity was achieved, where the "6" was the weight ratio of MCA to FR-PA6. The other samples with different weight contents of MCA were prepared according to the above procedure. Their relatively viscosities and viscosity average molecular weights were shown in Table 1.

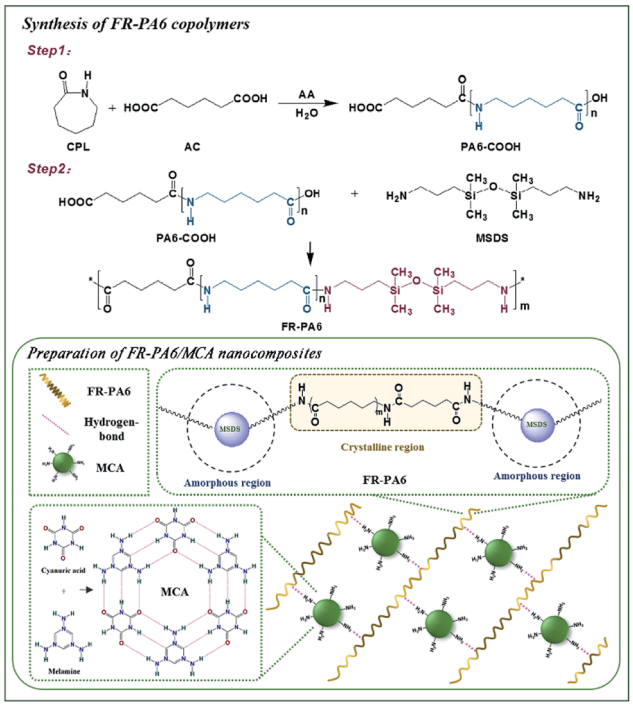

Fig. 1 Synthetic route of FR-PA6/MCA nanocomposites.

Measurements and characterization

The viscosity average molecular weights (M_η) of the samples were determined by equation:

$$[\eta] = kM_\eta^{\alpha} \quad (1)$$

where intrinsic viscosity $[\eta]$ was measured in *m*-cresol with a concentration of 0.005 g mL^{-1} at 25 °C ($\alpha = 0.61$ and $k = 240 \times 10^{-3}$) according to ISO 3105. The $[\eta]$ was measured at least 5 times and the variation coefficient was less than 1%. Fourier transform infrared (FTIR) spectra were recorded on a PerkinElmer spectrum one spectrometer with wavenumbers of 400 to 4000 cm^{-1}. ^{1}H and ^{29}Si nuclear magnetic resonance (NMR) spectra were recorded on an Avance 3HD 600 MHz NMR spectrometer (solvent: DMSO-d_6). Differential scanning calorimetry (DSC) curves were collected on a PerkinElmer thermal analyses instrument under nitrogen atmosphere. A 5 mg sample was first heated to 270 °C at 20 °C min^{-1} and kept in isothermal conditions for 3 min to remove the thermal history, and then was cooled to −30 °C at 20 °C min^{-1}. Afterward the sample was heated again to 370 °C at 10 °C min^{-1}. Thermogravimetric analysis (TGA) measurements were performed on a PerkinElmer thermal analyses instrument at a heating rate of 10 °C min^{-1} ranging from 30 to 700 °C under nitrogen atmosphere. X-ray diffraction (XRD) patterns were monitored using a Rigaku D/Max-2550 PC XRD analyser equipped with Cu-Kα ($\lambda = 0.154056$ nm) radiation. The limiting oxygen index (LOI) value was estimated by a ZR-1 instrument (Shanfang instrument Co., Ltd, China) with specimen dimensions of 100 × 6.3 × 3 mm^3 according to ASTM D2863-10. The vertical flame test

Table 1 List of FR-PA6, PA6/MCA and FR-PA6/MCA nanocomposites

Samples	MSDS (wt%)	PA6 (g mol^{-1})	MCA (wt%)	η (mL g^{-1})	M_η (g mol^{-1})
PA6	0	18 000	—	94.61	1.80×10^4
FR-PA6-3	3	8000	—	101.23	2.01×10^4
FR-PA6-6	6	4000	—	97.87	1.91×10^4
FR-PA6-9	9	2400	—	87.01	1.57×10^4
FR-PA6-12	12	1800	—	75.31	1.24×10^4
FR-PA6-15	15	1400	—	69.92	1.10×10^4
FR-PA6-9/MCA-6	9	2400	6	79.05	1.34×10^4
FR-PA6-9/MCA-8	9	2400	8	79.81	1.36×10^4
FR-PA6-9/MCA-10	9	2400	10	80.12	1.37×10^4
PA6/MCA-6	0	18 000	6	88.65	1.62×10^4
PA6/MCA-8	0	18 000	8	89.23	1.64×10^4
PA6/MCA-10	0	18 000	10	89.31	1.64×10^4
FR-PA6-6/MCA-8	6	4000	8	96.26	1.85×10^4
FR-PA6-12/MCA-8	12	1800	8	70.32	1.27×10^4

(UL-94) was carried out by CFZ-II burning tester (Jiangning Analysis Instrument Co., China) with 130 × 10 × 3.2 mm^3 by ASTM D3801. The melt droplets were averaged by 5 specimens from the real-time combustion test with specimen dimensions of 100 × 6.3 × 3 mm^3. A microscale combustion calorimeter (MCC, Govmark) was used to characterize the combustion behaviour according to ASTM D7309-7. A 6–10 mg sample was heated to 900 °C from 30 °C with a heating rate of 1 °C s^{-1}. The pyrolysis-gas chromatography/mass spectrometry (Py-GC/MS) testing was performed on a Shimadzu GC/MS-QP-2010 Ultra spectrometer. Tensile properties were measured on a CMT-4104-BZ-MTS universal testing machine with a speed of 50 mm min^{-1} by ASTM D412. Morphologies of residues were characterized by scanning electron microscopy (SEM) on VEGA3 TESCAN GMH/GMU.

Results and discussion

Chemical structure

The structural characterization of FR-PA6 is shown in Fig. 2. From the FTIR spectrum of FR-PA6 in Fig. 2(a), the characteristic absorption peaks assigned to the stretching of Si–O–Si and Si–C (MSDS) were observed at 1069 cm^{-1} and 835 cm^{-1}, while the stretching vibration of carbonyl group (C=O) at 1712 cm^{-1} had disappeared, suggesting that a reaction occurred between PA6-COOH and MSDS. In Fig. 2(b), the protons of the MSDS moiety at (b) 2.9 ppm, (c) 1.9 ppm, (d) 0.5 ppm, and (e) 0.1 ppm are presented, and there is only one strong resonance peak for the FR-PA6 copolymers at the same chemical shift (δ = 7.2 ppm) in Fig. 2(c) of ^{29}Si NMR, which could be ascribed to the M^1 structure which represented the completely condensed silicon atom bonded with a siloxane bond.[21] Thus the conclusion that the FR-PA6 copolymer was synthesized successfully could be drawn.

Crystalline structure

Crystalline structure as a crucial index for semi-crystalline polymers was evaluated by XRD measurements. In Fig. 2(d–f), the main diffraction peaks of FR-PA6 and FR-PA6/MCA nanocomposites were presented in the same position at 2θ = 20.1° and 23.8°, corresponding to (200) and (002 and 220) reflections in α-form crystals of PA6.[22–24] But the crystallinities of the FR-PA6 copolymers and FR-PA6/MCA-8 composites were both reduced with the increasing MSDS content (Table S1†), which could be attributed to the destruction of the crystal perfection due to the introduction of MSDS and the reduced chain length of the PA6 segments.[25] Inversely, the addition of MCA nanoparticles increased the crystallinities of the FR-PA6-9/MCA nanocomposites from 41.6% to 47.8%. Meanwhile, all the FR-PA6/MCA-8 nanocomposites had a higher crystallinity (35.0%, 45.6%, and 54.5%) than the corresponding FR-PA6 copolymers (32.3%, 38.4%, and 46.7%), which was mostly attributed to the heterogeneous nucleation due to the introduction of the MCA nanoparticles.[2]

Thermal properties

The DSC curves of the prepared samples are shown in Fig. 3(a and b). The melting temperature (T_m) of FR-PA6 was apparently increased to 215 °C from 175 °C with the increasing molecular chain length of PA6. Simultaneously, a wide melting range was observed in FR-PA6, and the range broadened with the increasing content of MSDS owing to the destruction of crystal perfection for PA6 segments. Interestingly, multiple melting peaks were found in FR-PA6 with relatively low MSDS contents, probably resulting from the co-existence of the good crystallization and incomplete crystallization.[25] For FR-PA6/MCA, there was no obvious change on T_m, whereas the crystallization temperature (T_c) determined from the exothermic peak of the nanocomposites (164 °C) was higher than that of FR-PA6-9 (138 °C) in Fig. 3(c). This result can be ascribed to heterogeneous nucleation since the MCA nanoparticles alter the crystallization rate, crystal density and grain size of the matrix.[2]

TGA curves and the relative parameters are depicted in Fig. 3(d–f) and Table S1.† The temperature that weight loss is 5 wt% ($T_{5\%}$) was considered as the initial decomposition temperature, while the T_{max} was defined as the temperature of the sample maximal mass loss rate. It was clear that the introduction of MSDS made no difference to the thermal degradation mode but increased the char residues of FR-PA6 from 0.5% to 3.8% (Table S1†) since the silicon in MSDS with low surface

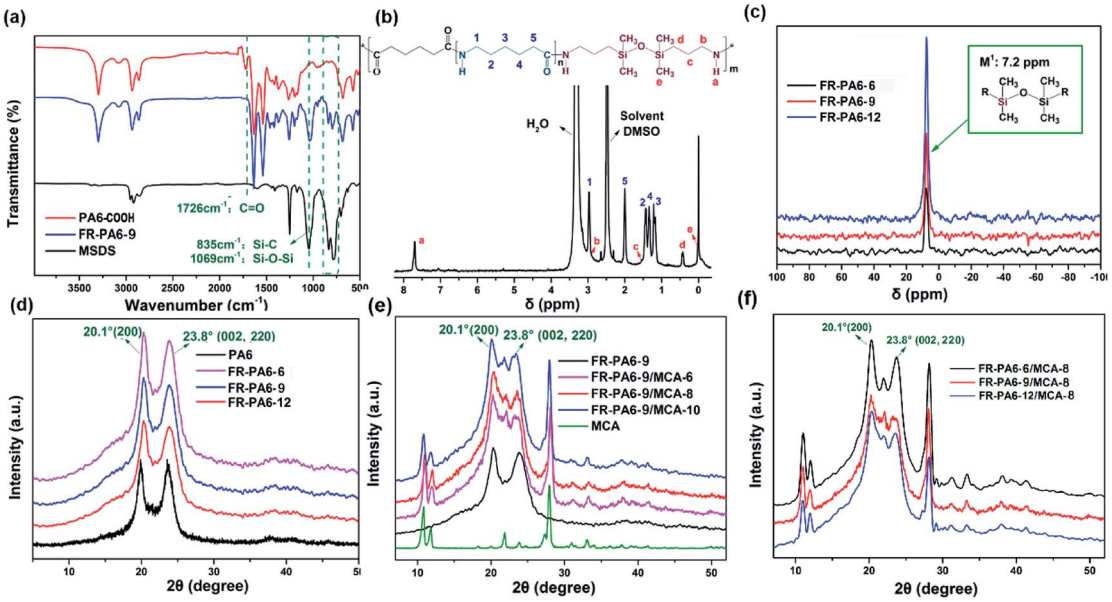

Fig. 2 (a) FTIR, (b) ^{1}H NMR, and (c) ^{29}Si NMR curves of FR-PA6, XRD curves of (d) FR-PA6, (e) FR-PA6-9/MCA and (f) FR-PA6/MCA-8 nanocomposites.

energy could transfer to the matrix surface and form a network structure of Si–O–Si and Si–C on the surface of the matrix, which isolated the external combustible gases, slowed down the further loss of carbon, and caught and immobilized more carbon to be carbonized.[26] When MCA nanoparticles were added, the degradation behaviours of the nanocomposites distinctly changed to a two-stage degradation mode, and the values of $T_{5\%}$ and T_{max} were sharply decreased to 331 °C and 348 °C of FR-PA6-9/MCA owing to the earlier degradation of MCA.[27] However, the T_{max2} values of these nanocomposites exceeded the T_{max} value of FR-PA6-9 (462 °C), suggesting the pyrolysis process of the matrix was delayed under the action of MCA.

Flame retardancy

UL-94 and LOI tests are two classical methods for estimating the combustion of materials in real fires, and the corresponding results are listed in Table 2. Obviously, the level of the UL-94 test for PA6 was no rating (NR), while FR-PA6 copolymers passed the UL-94 V-2 rating with extremely reduced melting droplet amounts. The real-time combustion results confirmed the reduction of melt droplets visually in Fig. S1.†

Results showed that FR-PA6-9 was extinguished after 6 melt droplets dropped, while PA6 kept burning with serious dripping after 30 s. Although both PA6/MCA-6 and FR-PA6-9/MCA-6 were ignited in air, the latter was self-extinguished after only 1

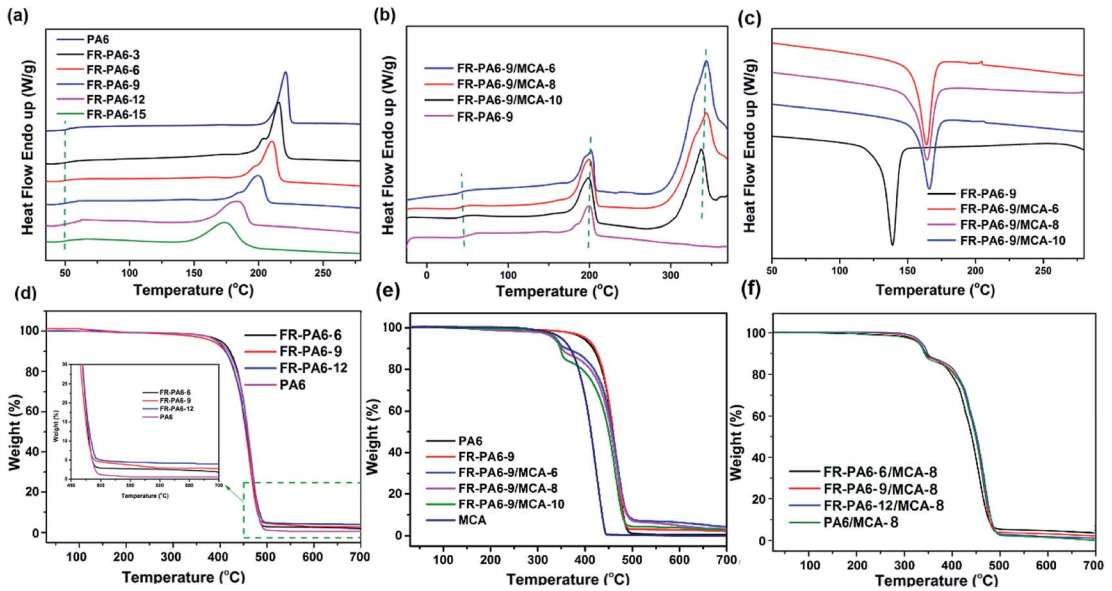

Fig. 3 DSC curves of (a) FR-PA6, (b and c) FR-PA6/MCA nanocomposites, TGA curves of (d) FR-PA6, (e) FR-PA6-9/MCA and (f) FR-PA6/MCA-8.

Table 2 Combustion data of PA6, FR-PA6 and FR-PA6/MCA nanocomposites[a]

Sample	UL-94 rating	Melting droplet amount	Burning drip	LOI (%)
PA6	NR	NC	Yes	21.5
FR-PA6-6	V-2	NC	Yes	22.5
FR-PA6-9	V-2	6.8	Yes	22.5
FR-PA6-12	V-2	5.4	Yes	22.0
PA6/MCA-6	V-2	3.8	Yes	25.7
PA6/MCA-8	V-2	3.3	Yes	28.0
PA6/MCA-10	V-0	2.1	No	30.8
FR-PA6-9/MCA-6	V-2	2.2	Yes	27.6
FR-PA6-9/MCA-8	V-0	1.5	No	29.2
FR-PA6-9/MCA-10	V-0	1.0	No	32.7
FR-PA6-6/MCA-8	V-2	2.8	Yes	28.3
FR-PA6-12/MCA-8	V-0	1.8	No	28.5

[a] NR: no rating and NC: not count.

droplet dropped at 14 s, while the former was continuously burning and dripping until 30 s. The results preliminarily presented the synergistic effects between MCA and MSDS on improving the flame retardancy of PA6. As shown in Fig. 4(a), there was only a slight increase on the LOI values of FR-PA6 and FR-PA6/MCA-8 with the increasing MSDS content. It is known that silicon plays a positive role in improving the flame retardancy of materials in the condensed phase, but the excessive superficial Si–O–Si aggregate structure likely gave rise to the release of interior abundant heat, and then the possibility of continuous burning was increased.[28] Nonetheless, the sustaining increased indexes of UL94 and the melt droplet amounts of FR-PA6/MCA-8 compared with PA6/MCA-8 (Table 2) still confirmed the superiority of MSDS in improving the flame retardancy.

In Fig. 4(b), a distinctly linear growth from 22.5% to 32.7% is found on the LOI values of FR-PA6-9/MCA with raising the MCA content. It proved that MCA served as the synergistic flame retardant of MSDS and was effective in strengthening the flame retardancy. Furthermore, the melt droplet amounts of the nanocomposites were diminished remarkably, and up to 8 wt% of MCA content, the V-0 rating of UL94 was passed (Table 2). Besides, FR-PA6-9/MCA proved superior to PA6/MCA with the same MCA contents on the values of LOI and UL94, reconfirming the assumption of the synergistic effects between MSDS and MCA.

MCC was an effective laboratory scale test to evaluate the flammability of polymers. Fig. 4(c) displays the heat release rate (HRR) curves of PA6, FR-PA6-9 and FR-PA6-9/MCA-10, and the corresponding parameters are listed in Table 3. The peak heat release rate (PHRR) value of PA6 quickly jumped to 565 W g^{-1} after it was ignited. By contrast, a sharp reduction on the PHRR value of 448 W g^{-1} appeared for FR-PA6-9 and 394 W g^{-1} for FR-PA6-9/MCA-10. Meanwhile, the total heat release (THR, 30.3, 26.5, 24.5 kJ g^{-1}) showed a similar variation to PHRR, which definitely demonstrated the significant impacts of MSDS and MCA on the flame retardancy of PA6.

Analysis of pyrolysis volatiles

The pyrolysis volatiles of samples were investigated by Py-GC/MS, and the total ion chromatograms (TIC) and the relevant MS results with the support of the NIST database of main pyrolysis products are shown in Fig. 5 and Tables S3–S7.† In Fig. 5(a), the volatile products of PA6 at 700 °C were mainly composed of carbon dioxide (CO_2, 1.44 min), butadiene (1.56 min), cyclopentadiene (1.97 min) and caprolactam (12.7 min). In contrast to PA6, there were three new peaks assigned to the linear siloxane compounds at 2.18, 4.47 and 6.29 min in the FR-PA6-9 spectrum at 700 °C from Fig. 5(b). Meanwhile, the proportion of caprolactam was decreased from 71.01% to 41.66% while the percentage of CO_2 was increased by over 4

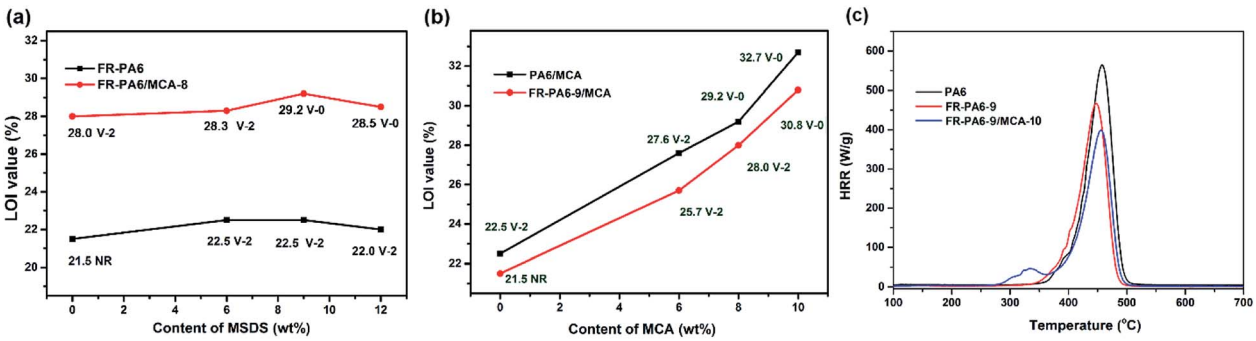

Fig. 4 LOI and UL94 values of FR-PA6/MCA with different contents of (a) MSDS and (b) MCA and the HRR curves of PA6, FR-PA6-9 and FR-PA6-9/MCA-10 (c).

Table 3 MCC combustion parameters of PA6, FR-PA6 and FR-PA6/MCA nanocomposites

Sample	HRC (J g^{-1} K^{-1})	PHRR (W g^{-1})	THR (kJ g^{-1})	T_{peak} (°C)
PA6	562	565	30.3	457.9
FR-PA6-9	470	448	26.5	457.8
FR-PA6-9/MCA-10	402	394	24.5	455.9

times. So it was deduced that the introduction of MSDS altered the pyrolysis process of PA6 in the gas phase. Meanwhile, it was clearly found that ME (16.27 and 20.49 min) and carbonitride (1.82 min) were the two major pyrolysis volatiles except for the CO_2 (1.44 min) for MCA at 700 °C from Fig. 5(c).

Pyrolysis volatiles of FR-PA6-9/MCA-10 at 350 and 700 °C were both checked to deeply investigate the synergetic influences of MCA and MSDS on thermal decomposition. As listed in Table S6,† the main products of nanocomposites at 350 °C were ME (16.59 min) and carbonitride (2.40 min) except for caprolactam, indicating that MCA had primarily decomposed. Besides, the appearance of caprolactam and a small quantity of silicon carbon fragments (23.975 min) meant that the molecular chains of the FR-PA6 matrix began to rupture at 350 °C, and a slightly crosslinking Si–O–Si structure was formed. According to Fig. 5(e), the peak of ME completely disappeared at 700 °C owing to the further pyrolysis of MCA by the heterocyclic nitrogen ring-opening reaction.[29] More cyclosiloxane and silicon–nitrogen compound volatiles were produced, such as hexamethylcyclotrisiloxane (5.46 min) and isocyanatotrimethylsilane (5.88 min). Compared with FR-PA6-9, the structure of silicon-containing pyrolysis volatiles was changed from a linear chain to a cyclic structure, suggesting the addition of MCA was beneficial to form more stable pyrolysis volatiles at high temperatures, contributing to the improvement of the flame retardancy of FR-PA6/MCA.

Analysis of residues

Analysis of the residues was important for studying the flame-retardant mechanism in the condensed phase. From the digital photos obtained after the LOI test in Fig. 6(a–c), there was an apparent white layer on the surface of FR-PA6 and FR-PA6/MCA residues, while almost no residue was observed for PA6. The morphologies of the corresponding residues were further monitored by SEM and are depicted in Fig. 6(a1–c2). In contrast from the smooth surface of the PA6 residues, the apparent residue sheet with some tiny cracks was seen in Fig. 6(b2) for FR-PA6, and the existence of the crack was perhaps the main reason for the limited flame retardancy of FR-PA6. For FR-PA6/MCA, many more residues were visually found, and the protective layer of the nanocomposites was denser and more complete as shown in Fig. 6(c1 and c2). It was known that the layer was conducive to retarding the transfer of combustible gases and heats, and creating an airtight space between matrix and barrier. When the interior oxygen and other combustible gases in this space were exhausted, the remnant heat could promote the matrix to form a stable carbon and carbonaceous-silicate structure, which effectively strengthened the protective barrier. Certainly, the structure was highly beneficial to the improvement of the anti-dripping property for samples. It was further verified that the addition of an appropriate amount of MCA helped to form a protective layer when MCA was incorporated with MSDS into PA6.

The chemical structures of the original FR-PA6-9/MCA-10, and the bottom and the top of the residues were characterized by FTIR and are displayed in Fig. 7(a). The peaks at 3418–3237 cm^{-1} and 1790–1733 cm^{-1} assigned to hydrogen bonds and NH_2 groups, respectively, disappeared in the curves of the bottom of residues, meaning that MCA was decomposed in advance and worked for enhancing the flame retardancy. Additionally, almost only two strong absorption peaks at 1040 cm^{-1} (Si–O–Si) and 810 cm^{-1} (Si–O–C) were seen in the curve of the top of residues, indicating that the superficial condensed phase was basically composed of SiO_2 and Si–C compounds. Comparing with the residues of FR-PA6-9/MCA-10, there was no distinct difference for FR-PA6-9 from Fig. 7(b). Therefore, this result verified that MSDS played a positive role in improving the flame retardancy of PA6 in the condensed phase rather than the MCA nanoparticles.

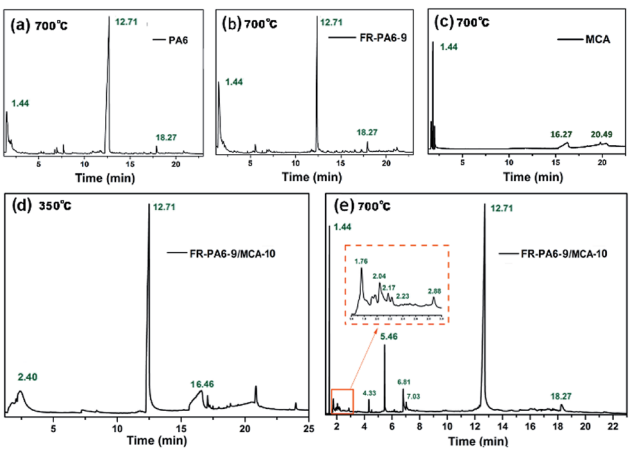

Fig. 5 TIC chromatograms from Py-GC/MS of (a) PA6, (b) FR-PA6-9, (c) MCA at 700 °C and FR-PA6-9/MCA-10 at (d) 350 °C and (e) 700 °C.

Illustration of the 'condensed-gas phase' flame-retardant mechanism

On the basis of the aforementioned analysis, the flame-retardant mechanism of FR-PA6/MCA nanocomposites is summarized in Fig. 8. At the initial heating stage, small molecular impurities, free and hydration water were decomposed and volatilized firstly.[2,8,29] When the temperature reached 350 °C, MCA as the main pyrolytic substance began to decompose. ME and some incombustible ammonia gases produced by

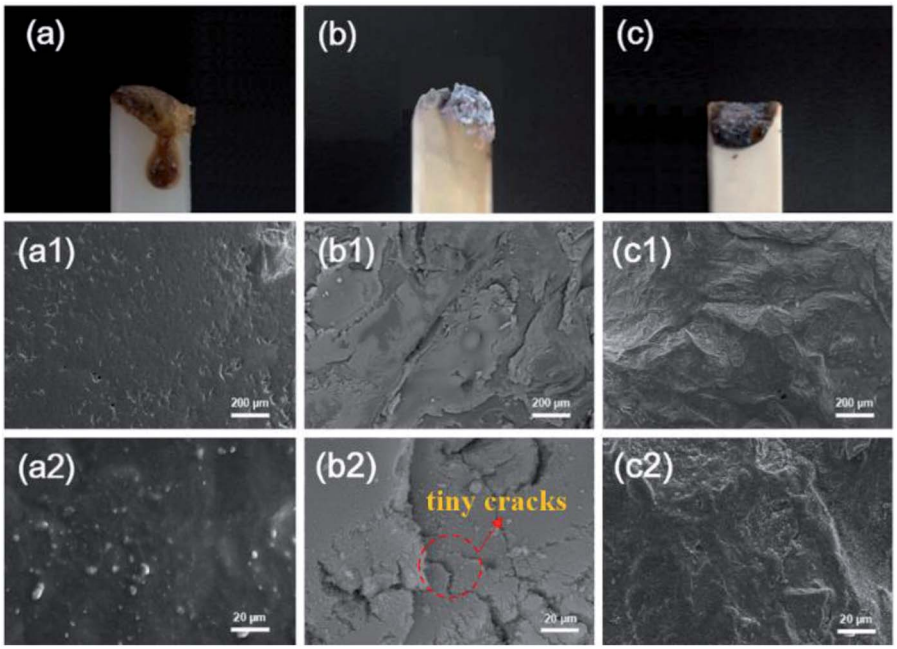

Fig. 6 Digital photos after the LOI test and SEM images of the residues after combustion for (a, a1, and a2) PA6, (b, b1, and b2) FR-PA6, and (c, c1, and c2) FR-PA6-9/MCA at different magnifications.

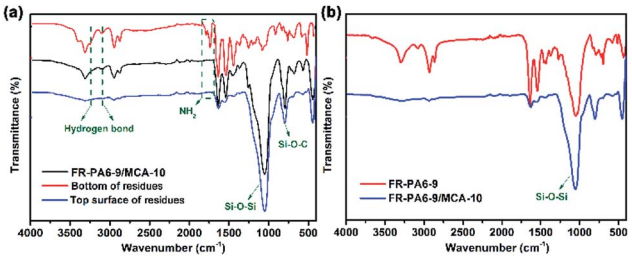

Fig. 7 FTIR spectra of (a) original, bottom of residues and top surface of residues for FR-PA6-9/MCA-10 and (b) the residues of FR-PA6-9 and FR-PA6-9/MCA-10 after LOI test.

the rupture of the hydrogen bond between the groups of C=O (CA) and N–H (ME) were released with huge heat dissipation. It was important for improving the flame retardancy by diluting the ignitable gases and reducing the environmental temperature effectively.[30] Subsequently, FR-PA6 and the decomposed ME were further degraded *via* a thermally induced chain scission reaction at higher temperatures. Herein, the released stabilized circular silicon volatiles and other incombustible volatiles were helpful to improve the flame retardancy in the gas phase. Specifically, the partially volatilized silicon could directly attach to the internal surface of the initial barrier, and then transformed to fumed silica. But large amounts of silicon were prone to remain in the condensed phase to form a compact and stable coking protective barrier (Si–C and Si–O–Si) on the surface of the matrix owing to its low surface energy.[31] The barrier not only isolated the underlying matrix from the external combustible gases and thermal feedback, hindered the escape of pyrolysis volatile gases, and caused the formation of thicker char layers, but also restricted the motion of the polymer melts, and then enhanced the anti-dripping properties. Nonetheless, the excessive barriers limited the release of interior heat to increase the probability for continuous burning of the underlying matrix. Additionally, under the action of MCA, the FR-PA6 macromolecules were catalysed to smaller oligomers with reduced polymeric viscosity. When the critical viscosity was reached, the melting matrix dropped off with abundant interior heat being taken away, which made up for the insufficiency of MSDS. Hence, there was a check and balance relationship between MSDS and MCA, and it could be ascribed to a 'condensed-gas phase' synergistic flame retardant mechanism.

Tensile properties

The mechanical properties of FR-PA6/MCA nanocomposites are important in actual applications. Fig. 9 shows the tensile properties of PA6, FR-PA6 and FR-PA6/MCA. Interestingly, FR-PA6 had higher tensile stress than PA6, which was perhaps resulting from the increasing crystallinity. Moreover, all the FR-PA6 samples were superior to PA6 by over 4 times on the elongation at a break from 88% to 470% with the increasing MSDS content. Combined with the investigation of XRD and DSC, this alteration of FR-PA6 copolymers might be associated with the significantly reduced hydrogen bond density, destructed crystalline perfection and increased amorphous region.[2] In Fig. 9(b), with the loading of MCA nanoparticles, the initial modulus and tensile stress of FR-PA6-9/MCA were slightly increased, while the elongation at the break was reduced. The increased stiffness of FR-PA6-9/MCA was ascribed to the nucleation effects of MCA nanoparticles since the existence of amino groups in MCA nanoparticles disturbed the

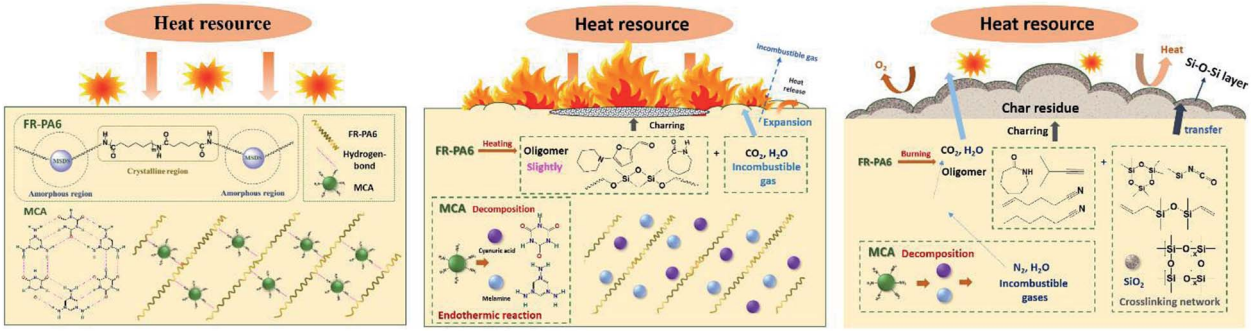

Fig. 8 Illustration of flame retardancy of FR-PA6/MCA nanocomposites.

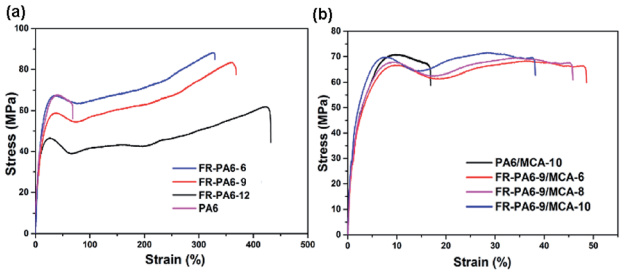

Fig. 9 Strain–stress curves of (a) FR-PA6 and (b) FR-PA6-9/MCA nanocomposites.

intermolecular bonds of FR-PA6 and enhanced the interaction forces between FR-PA6 macromolecular chains by forming stronger hydrogen bonds.[20] The reduction of the elongation at the break of FR-PA6-9/MCA could be interpreted as because MCA nanoparticles filled the clearances among molecular chains to limit the movements of the segments and separate the intertwining of molecular chains.[27] It is noteworthy that even though the tensile stresses and elongation at the break for FR-PA6-9/MCA nanocomposites were lower than FR-PA6-9 (83.5 MPa, 368%), they were still nearly identical to PA6 (64.4 MPa, 88%), indicating that the FR-PA6/MCA nanocomposites still kept the similar mechanical properties to PA6 despite the fact that the addition of MCA deteriorated the mechanical property of the nanocomposites.

Conclusions

In summary, eco-friendly and persistently silicon-containing inherent flame-retardant FR-PA6 copolymers were first synthesized by introducing MSDS into PA6 backbones *via* a controllable amidation reaction. Subsequently, FR-PA6/MCA nanocomposites were prepared by adding MCA nanoparticles into FR-PA6. Compared with PA6, the flame retardancy and mechanical properties of the synthesized FR-PA6 copolymers were extremely improved. The introduction of MSDS not only insulated the external combustible environment and restrained the motion of the polymer chains by forming a physical barrier, but also enhanced the tensile properties of the prepared FR-PA6. The prepared FR-PA6/MCA exhibited better flame retardancy with a LOI value of 32.7%, a UL94 V-0 level with only 1 melting droplet and a sharply diminished PHRR value. Meanwhile, the nanocomposites still maintained similar mechanical properties to PA6 even though the addition of MCA deteriorated the mechanical properties of the matrix. Accordingly, a special 'condensed-gas phase' synergistic flame-retardant mechanism of the FR-PA6/MCA nanocomposites was proposed. This work provided a facile route of 'copolymerization/blending' as a model for developing PA6 for diverse engineering applications.

Conflicts of interest

There are no conflicts to declare.

Acknowledgements

This work was financially supported by the National Key Research and Development Program of China (2016YFB0302700), Intelligent Manufacturing Program of China and the Fundamental Research Funds for the Central Universities (CUSF-DH-D-2018037).

Notes and references

1 H. Ge, G. Tang, W. Hu, B. Wang, Y. Pan, L. Song and Y. Hu, *J. Hazard. Mater.*, 2015, **294**, 186.
2 X. Feng, X. Wang, W. Cai, N. Hong, Y. Hu and K. Liew, *J. Hazard. Mater.*, 2016, **320**, 252.
3 H. Ma, L. Tong, Z. Xu and Z. Fang, *Adv. Funct. Mater.*, 2008, **18**, 414.
4 J. Jing, Y. Zhang, Z. Fang and D. Wang, *Compos. Sci. Technol.*, 2018, **165**, 161.
5 L. Zuo, W. Fan, Y. Zhang, L. Zhang, W. Gao, Y. Huang and T. Liu, *Compos. Sci. Technol.*, 2018, **139**, 57.
6 K. Sha, Y. Hu, Y. Wang and R. Xiao, *Mater. Res. Innovations*, 2014, **18**, 843.
7 X. Dong, L. Chen, R. Duan and Y. Wang, *Polym. Chem.*, 2016, **7**, 2698.
8 J. Sahyoun, V. Bounor-Legaré, L. Ferry, R. Sonnier, F. Da Cruz-Boisson, F. Melis, A. Bonhommé and P. Cassagnau, *Eur. Polym. J.*, 2015, **66**, 352.
9 L. Gua, J. Qiu, Y. Yao, E. Sakaib and L. Yang, *Compos. Sci. Technol.*, 2018, **161**, 39.

10 B. Chen, W. Gao, J. Shen and S. Guo, *Compos. Sci. Technol.*, 2014, **93**, 54.
11 J. Chen, S. Liu and J. Zhao, *Polym. Degrad. Stab.*, 2011, **96**, 1508.
12 A. Šehić, B. Tomšič, I. Jerman, J. Vasiljević, J. Medved and B. Simončič, *Polym. Degrad. Stab.*, 2016, **128**, 245.
13 S. Deh, F. Gähr and M. R. Buchmeiser, *Polym. Degrad. Stab.*, 2016, **130**, 155.
14 M. Long, S. Peng, W. Deng, X. Miao, N. Wen, Q. Zhou, X. Yang and W. Deng, *J. Mater. Chem. A*, 2017, **5**, 22761.
15 U. Eduok, O. Faye and J. Szpunar, *Prog. Org. Coat.*, 2017, **111**, 124.
16 W. Li, J. Chu, L. Heng, T. Wei, J. Gu, K. Xi and X. Jia, *Polymer*, 2013, **54**, 4909.
17 F. Liao, L. Zhou, Y. Ju, Y. Yang and X. Wang, *Ind. Eng. Chem. Res.*, 2014, **53**, 10015.
18 Y. Li, Y. Lin, K. Sha and R. Xiao, *Text. Res. J.*, 2016, **87**, 561.
19 Y. Chen, Q. Wang, W. Yan and H. Tang, *Polym. Degrad. Stab.*, 2006, **91**, 2632.
20 Y. Liu and Q. Wang, *J. Polym. Res.*, 2009, **16**, 583.
21 L. Z. Guan, J. F. Gao, Y. B. Pei, L. Zhao, L. X. Gong, Y. J. Wan, H. Zhou, N. Zheng, X. S. Du and L. B. Wu, *Carbon*, 2016, **107**, 573.
22 C. Ramesh and B. Gowd, *Macromolecules*, 2001, **34**, 3308.
23 J. Pepin, V. Miri and J.-M. Lefebvre, *Macromolecules*, 2016, **49**, 564.
24 J. Ho and K. Wei, *Macromolecules*, 2000, **33**, 5181.
25 Y. Zhang, H. Fan and B. G. Li, *J. Appl. Polym. Sci.*, 2011, **131**, 17.
26 R. Wang, D. Zhuo, Z. Weng, L. Wu, X. Cheng, Y. Zhou, J. Wang and B. Xuan, *J. Mater. Chem. A*, 2015, **3**, 9826.
27 J. Cai, A. Wirasaputra, Y. Zhu, S. Liu, Y. Zhou, C. Zhang and J. Zhao, *RSC Adv.*, 2017, **7**, 19593.
28 P. Kiliaris, C. D. Papaspyrides, R. Xalter and R. Pfaendner, *Polym. Degrad. Stab.*, 2012, **97**, 1215.
29 M. Coquelle, S. Duquesne, M. Casetta, J. Sun, X. Gu, S. Zhang and S. Bourbigot, *Polymers*, 2015, **7**, 316–332.
30 C. Isbasar and J. Hacaloglu, *J. Anal. Appl. Pyrolysis*, 2012, **98**, 221.
31 Y. Wang, X. Yang, H. Peng, F. Wang, X. Liu, Y. Yang and J. Hao, *ACS Appl. Mater. Interfaces*, 2016, **8**, 9925.